Numerical Evaluation of Load-Displacement Relationships for Non-Slender Monopiles in Sand

Sørensen, Søren Peder Hyldal; Møller, M.; Brødbæk, K. T.; Augustesen, Anders Hust; Ibsen, Lars Bo

Publication date:
2009

Document Version
Publisher's PDF, also known as Version of record

Numerical Evaluation of Load-Displacement Relationships for Non-Slender Monopiles in Sand

S. P. H. Sørensen
M. Møller
K. T. Brødbæk
A. H Augustesen
L. B. Ibsen

ISSN 1901-726X
DCE Technical Report No. 80

AALBORG UNIVERSITY
Department of Civil Engineering

Aalborg University
Department of Civil Engineering
Water & Soil

DCE Technical Report No. 80

Numerical Evaluation of Load-Displacement Relationships for Non-Slender Monopiles in Sand

by

S. P. H. Sørensen
M. Møller
K. T. Brødbæk
A. H. Augustesen
L. B. Ibsen

December 2009

Scientific Publications at the Department of Civil Engineering

Technical Reports are published for timely dissemination of research results and scientific work carried out at the Department of Civil Engineering (DCE) at Aalborg University. This medium allows publication of more detailed explanations and results than typically allowed in scientific journals.

Technical Memoranda are produced to enable the preliminary dissemination of scientific work by the personnel of the DCE where such release is deemed to be appropriate. Documents of this kind may be incomplete or temporary versions of papers—or part of continuing work. This should be kept in mind when references are given to publications of this kind.

Contract Reports are produced to report scientific work carried out under contract. Publications of this kind contain confidential matter and are reserved for the sponsors and the DCE. Therefore, Contract Reports are generally not available for public circulation.

Lecture Notes contain material produced by the lecturers at the DCE for educational purposes. This may be scientific notes, lecture books, example problems or manuals for laboratory work, or computer programs developed at the DCE.

Theses are monograms or collections of papers published to report the scientific work carried out at the DCE to obtain a degree as either PhD or Doctor of Technology. The thesis is publicly available after the defence of the degree.

Latest News is published to enable rapid communication of information about scientific work carried out at the DCE. This includes the status of research projects, developments in the laboratories, information about collaborative work and recent research results.

Published 2009 by
Aalborg University
Department of Civil Engineering
Sohngaardsholmsvej 57,
DK-9000 Aalborg, Denmark

Printed in Aalborg at Aalborg University

ISSN 1901-726X
DCE Technical Report No. 80

Numerical Evaluation of Load-Displacement Relationships for Non-Slender Monopiles in Sand

S. P. H. Sørensen; M. Møller; K. T. Brødbæk; A. H. Augustesen; and L. B. Ibsen

Abstract

Monopiles are an often used foundation concept for offshore wind turbine converters. These piles are highly subjected to lateral loads and thereby bending moments due to wind and wave forces. To ensure enough stiffness of the foundation and an acceptable pile-head deflection, monopiles with diameters of 4 to 6 m are typically necessary. In current practice these piles are normally designed by use of the p–y curve method although the method is developed and verified for slender piles with diameters up to approximately 2 m. This paper treats numerical models constructed in the commercial programs *FLAC*^{3D} and *Plaxis 3D Foundation* with the objective to examine horizontally loaded, large-diameter piles in cohesionless soil. First, the models are calibrated to six small-scale tests conducted in a pressure tank. Hereafter, the models are extended to large-scale simulations. The large-scale simulations are evaluated with the following main findings: Non-slender piles behave almost rigidly when subjected to lateral loads implying a significant deflection at the pile-toe; the initial stiffness of the p–y curves is found to increase for an increase in diameter; the initial stiffness of the p–y curves is independent of the embedded length of the pile and the pile bending stiffness; the initial stiffness of the p–y curves does not vary linearly with depth as suggested in the offshore design regulations; the Winkler model approach is found to provide reasonable results for large-diameter, non-slender piles if the initial stiffness is updated to vary by means of a power function.

Keywords: Monopile, Lateral load, p–y curves, Modulus of subgrade reaction, Winkler model approach, Sand, *FLAC*^{3D}, *Plaxis 3D Foundation*.

1 Introduction

In current design of laterally loaded monopiles, used as foundation for offshore wind turbines, the p–y curve method is normally employed. Two of the non-clarified parameters related to the expression for the p–y curves for piles in cohesionless soil is, cf. Brødbæk et. al (2009):

- Slenderness ratio L/D
- Initial stiffness of the p–y curves

Monopile foundations for modern offshore wind turbines have $L/D < 10$ and behave as almost rigid objects when subjected to lateral loads. In contrast the p–y curves employed in the design regulations, e.g. API (1993) and DNV (1992), are based on testing of two slender flexible piles with $L/D = 34.4$, cf. Cox et al. (1974).

The initial stiffness of the p–y curves is considered independent of the pile properties among these the pile diameter, which seems questionable. The research within the field of effects of pile diameter on the initial stiffness gives contradictory conclusions as described by Brødbæk et. al (2009).

As large-scale tests are expensive and time consuming a proper numerical model cali-

brated to small-scale tests is an important tool in the assessment of the p–y curve method. This paper describes numerical models constructed in the commercial programs *FLAC*^{3D} and *Plaxis 3D Foundation* with the objective to examine horizontally loaded, large-diameter piles in cohesionless soil. For offshore wind turbine foundations only small deformations are allowed. On this basis, the focus of the analysis is the initial stiffness of the p–y curves. The outline of the paper is as follows:

- **Laboratory test setup:** The test setup forming the basis for the calibration of the numerical models is presented. The tests are carried out in a pressure tank in order to minimise the scale effects attached to small-scale tests at 1-g.
- **Construction of 3D models:** The model conducted in *FLAC*^{3D} is first calibrated to the small-scale laboratory tests and hereafter extended to large-scale. In order to validate the results provided by *FLAC*^{3D} a comparable model is created in *Plaxis 3D Foundation*.
- **Calibration of numerical models:** The *FLAC*^{3D} model is successfully calibrated to the results obtained in the laboratory tests. From this calibration the interface properties are determined. The *Plaxis 3D Foundation* does not fit the test results satisfactory. The tendencies from varying the diameter however, are similar for the two numerical models.
- **Simulation of large-scale monopiles:** The calibrated numerical models are extended to simulate large-scale offshore monopiles with diameters of $D = [2,3,5,7]$ m.
- **Comparison of *FLAC*^{3D} with a Winkler model approach:** The Winkler model approach incorporating the API p–y curves is evaluated against the soil-pile interaction obtained by means of *FLAC*^{3D}.

2 Laboratory test setup

Six quasi-static laboratory tests have been conducted on two instrumented closed-ended aluminium pipe piles with outer diameters, D, of 60 mm and 80 mm, respectively. The wall thickness is 5 mm. Both piles have a slenderness ratio $L/D = 5$ corresponding to an embedded length, L, of 0.3 and 0.4 m, respectively. The piles are subjected to a horizontal load applied 0.370 m above the soil surface. The piles are instrumented with strain gauges in five levels beneath the soil surface, cf fig. 1. Furthermore, displacement transducers are attached to the pile at 200 mm, 370 mm, and 480 mm above the soil surface.

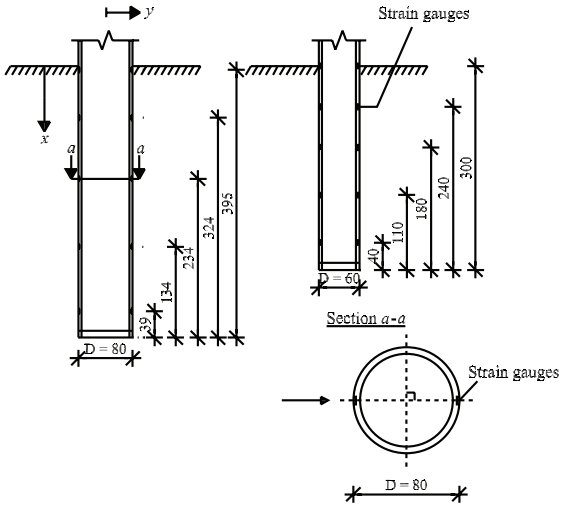

Figure 1: Strain gauge levels. Measures are in mm.

In order to overcome sources of error such as small non-measurable stresses, a non-linear failure criterion, and excessive angles of internal friction, the piles are installed and tested in a pressure tank containing 0.69 m of fully saturated sand. The stress dependent angle of internal friction and Young's modulus of elasticity are determined from cone penetration tests, in accordance to Ibsen et al. (2009). A pic-

ture of the pressure tank is shown in fig. 2.

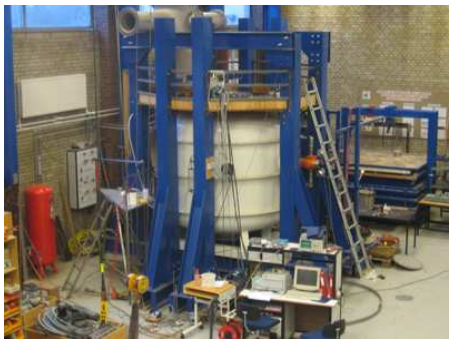

Figure 2: Pressure tank.

In the pressure tank an elastic membrane is placed on the soil surface, leaving the soil sealed from the top part of the tank. The pile is lead through a sealing in the elastic membrane allowing the pile to be extended above the soil surface. When increasing the air pressure in the upper part of the tank, the elastic membrane is pressed against the soil, by which the stresses in the soil are increased. The lower part of the tank, containing the saturated soil, is connected to an ascension pipe, leaving all the applied loads to pressure between the grains, i.e. an increase in effective stresses. The details of the laboratory tests are described by Sørensen et. al (2009). The material properties of the soil and the piles for the six tests are listed in the appendix.

3 Construction of 3D models

The numerical models are at first constructed to match the laboratory tests in scale 1:1 in order to calibrate the interface properties and validate the models. After a calibration to the laboratory tests the models are extended to large-scale offshore wind turbine foundations, at which the effect of pile diameter on initial stiffness is analysed.

3.1 *FLAC*^{3D}

A three-dimensional numerical model is constructed in $FLAC^{3D}$, which is a commercial program based on a dynamic explicit finite difference solver. To simplify the model, symmetry of the test setup is utilised, so only one half of the pile and surrounding soil are modelled. Furthermore, the pile is modelled as a solid cylinder, in contrast to the closed-ended pipe piles employed in the laboratory tests. The geometry and the orientation of the coordinate system is shown in fig. 3. A finer mesh discretisation is employed in the soil near the pile, as large variations in strains and stresses occurs in this area.

The bending stiffness of the solid pile in the numerical model is given as an equivalent to the stiffness of the hollow test pile, resulting in a reduced Young's modulus of elasticity given as:

$$E_{solid} = \frac{E_{hollow} I_{hollow}}{I_{solid}} \qquad (1)$$

The subscripts *hollow* and *solid* denote the parameters derived for the pipe piles, in this case the laboratory test piles and large-scale piles, and the parameters employed in the $FLAC^{3D}$ model, respectively. The weight of the hollow and the solid piles are in the same way equivalented. Poisson's ratio of the pile material is not scaled, leading to an incorrect scaling of the shear modulus and bulk modulus. The effect of not scaling these parameters correctly is however considered negligible as the pile primarily is subjected to bending moments.

The grid is generated from simple zone elements. Each of these zones consist of five first order, constant rate of strain, tetrahedral subelements. The soil-pile interface is modelled by the standard $FLAC^{3D}$ interface consisting of triangular elements. By default two triangular interface elements are created for each zone face. The interfaces are one-sided and attached to the

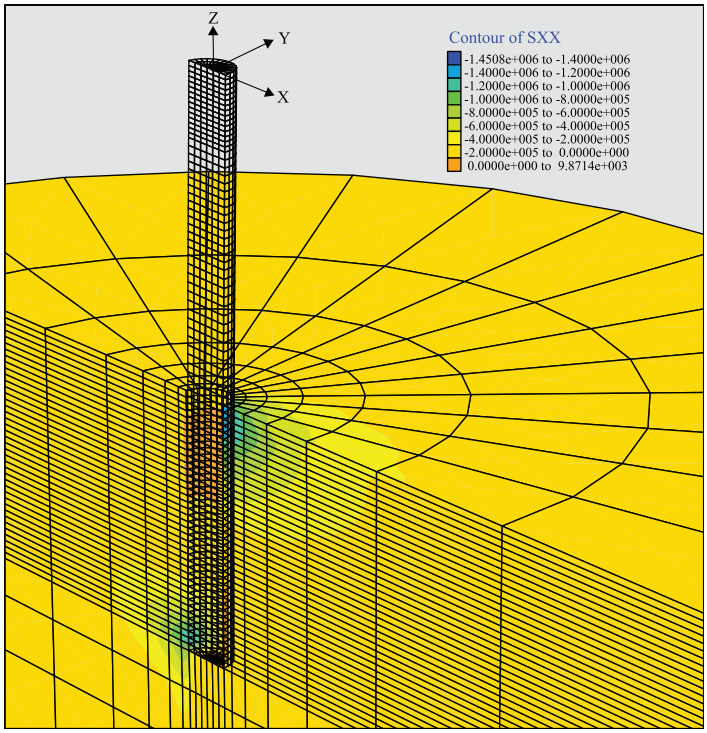

Figure 3: Three-dimensional mesh for the $FLAC^{3D}$ model and effective horizontal stresses in Pa, $SXX = \sigma'_{xx}$, (in the plane of symmetry) for a horizontal load at 5300 N, $D = 0.08$ m, $L = 0.4$ m, and an overburden pressure of $P_0 = 100$ kPa.

soil. For the constitutive relations of the interfaces a linear Coulomb shear-strength criterion is employed.

At the outer perimeter of the soil, the element nodes are restrained in the x and y directions. At the bottom surface the nodes are restrained in all directions while the surface at the symmetric line is restrained in the y direction. The outer boundaries are adjusted to each pile diameter and pile length as given in section 3.3.

The horizontal load is applied as horizontal node velocities acting with a given vertical eccentricity. The horizontal velocities are applied at the nodes corresponding to $x = 0$ at the pile-head acting in the positive x-direction. Hereby, no artificial bending moment is introduced at the pile-head. It should be emphasised that for $D = 2$ m the simulation did not reach equilibrium for the displacement controlled model. This might be due to the ratio between load eccentricity and pile diameter causing dynamic effects to influence the calculation. Instead the horizontal load was applied as nodal forces acting at the pile-head for $D = 2$ m. It has been validated that the two methods for applying the horizontal load produce similar results with only small deviations, cf. fig. 4.

Disagreement between the applied load and the bending moment of the pile at the soil surface has been observed when modelling the pile with only few elements in the vertical direction. A relatively fine discretisation is therefore employed for the pile to ensure convergence of the stresses. An example of the agreement between the applied load and the computed bending moment in the pile at the soil surface is shown in fig. 5.

When creating the model, the soil elements are generated at first. Secondly, the interfaces are generated and attached to

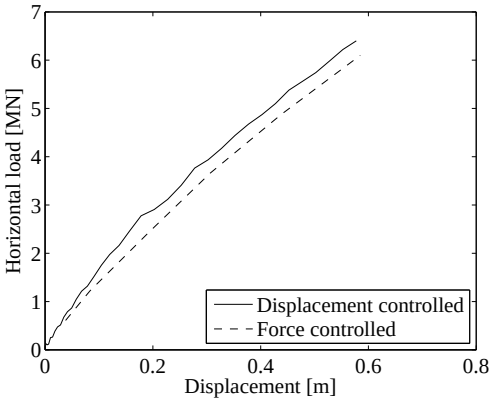

Figure 4: Load-displacement relationships for $D = 3$ m, and $L = 20$ m obtained from the displacement controlled and load controlled models, respectively.

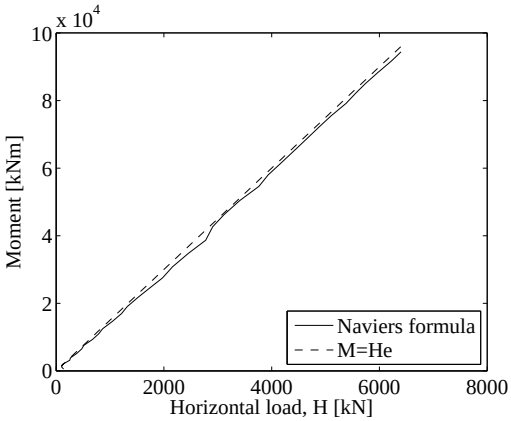

Figure 5: Comparison of the horizontal load, H, multiplied with the load eccentricity, e, with the bending moment at the soil surface calculated as presented in section 3.6 for $D = 3$ m, and $L = 20$ m. The pile has in the vertical direction been divided into 40 elements beneath the soil surface and 50 elements above the soil surface.

the soil elements. Thirdly, the pile is generated. The pile is generated above the soil surface and afterwards moved into the soil. Hereby, it is possible to group the pile elements and to specify pile nodes for the computation of bending moment.

The calculations are executed in steps. Firstly, the initial stresses are generated using a K_0-procedure. Secondly, an equilibrium state is calculated where the pile as well as the soil are assigned the properties of the soil. Furthermore, the pile is assumed smooth at this stage, all in order to prevent stress concentrations near the pile. After the first equilibrium state the correct pile and interface properties are assigned and the model is brought to a second equilibrium state. Additionally, overburden pressure is for the small-scale tests applied as an initial load before the second equilibrium state. After reaching the second equilibrium state, velocities are applied to the pile-head in small increments in order to minimise inertial forces in the system.

3.2 *Plaxis 3D Foundation*

A three-dimensional model is constructed by means of the commercial program *Plaxis 3D Foundation*, which is based on the finite element method and developed to solve geotechnical problems. In contrast to $FLAC^{3D}$ a full model is constructed as *Plaxis 3D Foundation* does not facilitate the symmetrical conditions to be utilised. The pile is modelled as a hollow pile with use of wall elements. Wall elements are predefined eigth–noded quadrilateral plate elements. The wall elements can deform by shearing, bending, and axial deformation. In order to apply the lateral load equally to the pile-head nodes a rigid top plate is employed. The lateral load is applied as a point load in the centre node of the top plate. In order to compare the results from the two numerical models a plate is applied at the bottom of the pile. Both the top plate and the bottom plate is made of floor elements, which is a predefined plate element with six nodes. Similar to the wall element type, floor elements can deform by shearing, bending, and axial deformation. However, no interfaces are attached to the floor element type. Hereby, the footing of the pile and the soil are rigidly connected.

The soil is divided into clusters in order to employ a finer mesh in the area close to the pile. An example of the discretisation of a model is shown in fig. 6. Notice

that the coordinate system differs from the coordinate system employed in *FLAC*^{3D}, cf. fig. 3. The soil is divided into 15-noded wedge elements. All the elements provide a second-order interpolation of the displacements and correspondingly a first-order interpolation of stresses and strains.

Interface elements with 16 nodes, corresponding to eight pairs of nodes, are applied between the soil and the wall elements. The thickness of the interfaces are set to zero, however a virtual thickness is applied in order to establish the stiffness of the interface. The Coulomb criterion is employed for the interfaces to distinguish between elastic and plastic behaviour. The stiffness and strength of the interface is governed by the factor, R_{inter}. The angle of internal friction of the interface, φ_i, is set to the angle of internal friction of the soil, φ_{tr}, multiplied with R_{inter} while the stiffness parameters, E_i and G_i, are scaled with R_{inter} squared. Poisson's ratio is by default set to $\nu_i = 0.45$ in the interface. For a perfectly rough soil-structure interface $R_{inter} = 1.0$. As the transition between a soil and a structure is normally weaker and more flexible than the associated soil layer, values of $R_{inter} < 1.0$ should be applied.

The boundary conditions are similar to the ones employed in *FLAC*^{3D} except that no boundary restrictions are attached to the plane of symmetry. The size of the soil mass at each simulation is presented in section 3.3.

When computing the equilibrium state the K_0-procedure is employed. The equilibrium state is calculated in stages. Firstly, equilibrium is calculated for the model containing only soil. Secondly, a possible overburden pressure is applied as a vertical load. Thirdly, the pile is installed and a new equilibrium state is calculated. In order to obtain load-displacement relationships and p–y curves the total lateral load is applied in stages.

3.3 Outer boundaries

In order to avoid the outer boundaries from affecting the results, the volume of the soil is adjusted to each pile diameter. According to Abbas et al. (2008) the width of the soil mass should be $40D$ and the height of the soil mass should be $h = L + 20D$, where L denotes the embedded length of the pile and D denotes the pile diameter, cf. fig. 7. However, Abbas et al. (2008) investigated piles which were exposed to both horizontal and vertical loading. As only the behaviour due to lateral loading is examined in the simulations a smaller height of the soil mass is employed. For the large-scale simulations the width of the soil mass is set to $40D$ while the height is set to $L + 10$ m. The small-scale simulations are supposed to fit the laboratory tests. The outer boundaries are therefore given as the volume of the soil mass in the pressure tank, i.e. a diameter of 2.1 m and a soil depth of 0.69 m. *FLAC*^{3D} allows a curved outer boundary, which is utilised in all models. On the opposite, *Plaxis 3D Foundation* allows only a squared outer boundary why the diameter of the models in *FLAC*^{3D} corresponds to the side length in *Plaxis 3D Foundation*.

For both the model in *FLAC*^{3D} and *Plaxis 3D Foundation* it has been observed that the zone of failure does not reach the outer boundaries.

3.4 Material models

In both numerical models a traditional elasto-plastic Mohr–Coulomb model is employed to describe the constitutive relations. The yield function of the constitutive model is controlled by a non-associated flow rule. No tension forces are allowed in the soil, as a pure friction material is considered, why tension cut-off is appointed.

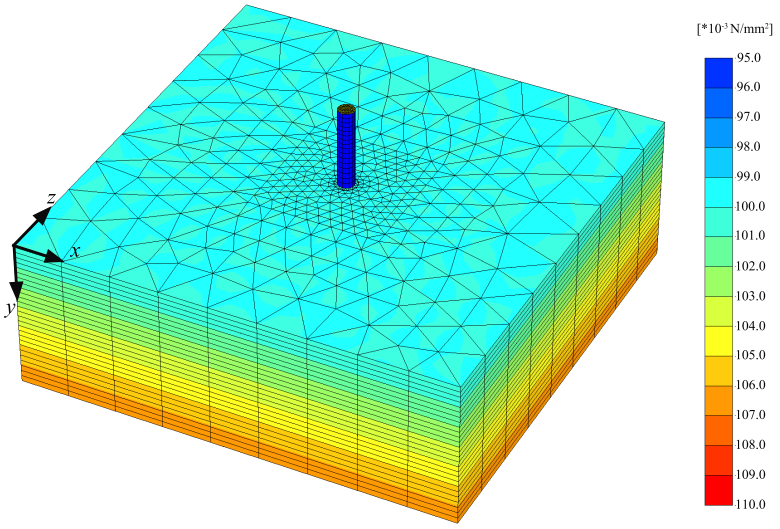

Figure 6: Three-dimensional mesh for the *Plaxis 3D Foundation* model and effective vertical stresses in MPa, σ'_{yy}, prior to the horizontal load is applied for $D = 0.08$ m, $L = 0.4$ m, and $P_0 = 100$ kPa.

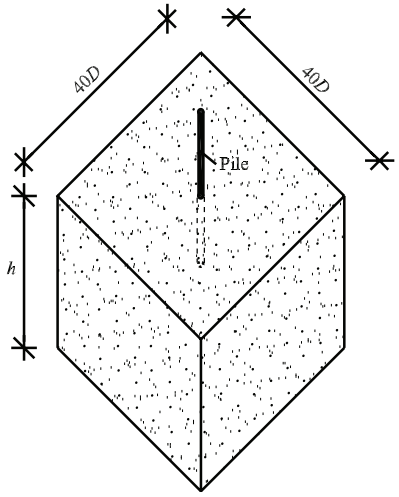

Figure 7: Dimensions of the soil volume. D is the outer diameter of the employed pile.

3.5 Young's modulus of elasticity, E_0

When calibrating the numerical models to the laboratory tests the soil parameters are assumed to remain constant with depth due to the small variations in effective stresses. Young's modulus of elasticity of the soil is however varied with respect to the stress level for the calculations on large-scale monopiles. The tangential Young's modulus of elasticity, E_0, is assumed to vary with the minor principal stress, σ'_3, on the basis of (2)-(3) as proposed by Ibsen et al. (2009). Equation (2)-(3) are valid for Baskarp Sand Nr. 15. The relative density, I_D, is inserted in % and $\sigma_3^{\prime ref}$ is a reference minor principal stress of 100 kPa.

$$E_0 = E_0^{ref} \left(\frac{c \cdot \cos(\varphi_{tr}) + \sigma'_3 \sin(\varphi_{tr})}{c \cdot \cos(\varphi_{tr}) + \sigma_3^{\prime ref} \sin(\varphi_{tr})} \right)^{0.58} \tag{2}$$

$$E_0^{ref} = 1.82(0.6322 I_D^{2.507} + 10920)[\mathrm{kN/m^2}] \tag{3}$$

For the model in *Plaxis 3D Foundation* the variation of Young's modulus is approximated by three stepwise linear functions. The tangential Young's modulus of elasticity of the soil according to (2)-(3) and the approximated stepwise functions are illustrated in fig. 8.

3.6 Computation of soil resistance and pile bending moment

The bending moment, M, at a given level of the pile is in $FLAC^{3D}$ calculated by use of Naviers formula:

$$M = \frac{(\sigma_{zz,i} - \overline{\sigma}_{zz,i}) I_{yy}}{x_i} \tag{4}$$

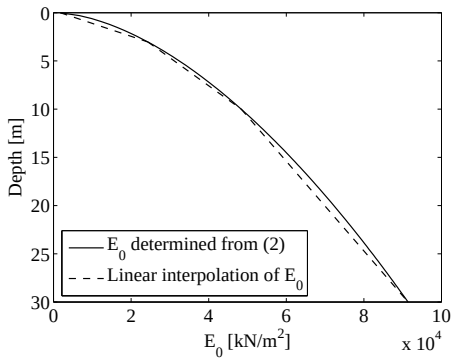

Figure 8: Variation of Young's modulus of elasticity of the soil, E_0.

where $\sigma_{zz,i}$ is the vertical normal stresses at point i, I_{yy} is the second moment of inertia around the y-axis, x_i is the x-coordinate of point i, and $\overline{\sigma}_{zz,i}$ is the average vertical stress corresponding to the axial force acting in the pile. The bending moment is calculated from two points ($y = 0, x = \pm D/2$) at each level of the pile in order to eliminate the average vertical stress.

For the model in *Plaxis 3D Foundation* the bending moment is computed by a summation of the product of the nodal forces in the y-direction, $f_{y,i}$, and the x-coordinates, for all nodes at a given level of the pile:

$$M = \sum_{i}^{n} f_{y,i} x_i \tag{5}$$

The soil resistance is for both numerical models calculated by differentiating the bending moment distribution along the pile twice. The double differentiation gives an amplification of errors in the bending moment distribution. In order to minimise these errors the piecewise polynomial curve fitting method described by Yang and Liang (2006) is employed. Hereby, the bending moment distribution is estimated by fitting five succesive moment data points to 3. order polynomials. It is emphasised that (4) and (5) are related to the coordinate systems employed in the respective models.

4 Calibration of numerical models

On the basis of the derived soil parameters given in the appendix the numerical models in *FLAC*^{3D} and *Plaxis 3D Foundation* have been calibrated. The soil parameters are assumed to be constant with depth.

4.1 *FLAC*^{3D}

In the calibration of the model constructed in *FLAC*^{3D} the obtained load-displacement relationship and bending moment distributions have been compared to the test results. As an example of the calibration the load-displacement relationship is shown in fig. 9 for $D = 80$ mm, and $P_0 = 100$ kPa. Figure 10 presents the calibrated and measured bending moment distribution at a horizontal load of 2100 N for the same test. As shown in fig. 9 and fig. 10, the agreement between the experimental and computed values is relatively good. Similar analyses have been made for the five remaining tests with similar results. As the computed values by means of *FLAC*^{3D}, when employing the soil parameters obtained from CPT's, are rather similar to the measured values it is concluded that the numerical model produce realistic results. The difference between the calibrated and measured load-displacement relationships and bending moment distributions might be due to uncertainties from determination of the soil parameters rather than numerical errors. In the calibrations the wall friction angle, δ, has been set to 30°, and the dilatancy angle to $\psi = 10°$. The shear stiffness, k_s, and the normal stiffness, k_n, of the interface has been set to $k_s = k_n = 100E_0$.

4.2 *Plaxis 3D Foundation*

In order to validate the results obtained by means of *Plaxis 3D Foundation* the pile

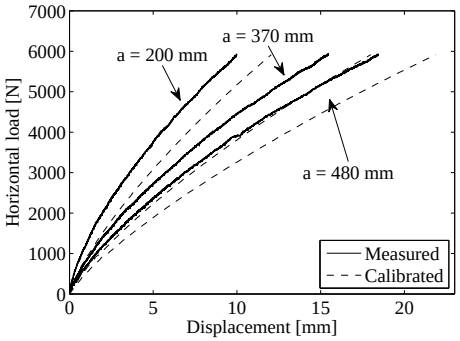

Figure 9: Calibrated load-displacement relationship determined by means of $FLAC^{3D}$ at three levels above soil surface, for the test with $D = 0.08$ m, $L = 0.4$ m, and $P_0 = 100$ kPa. a denotes the distance from the soil surface to the level of measuring.

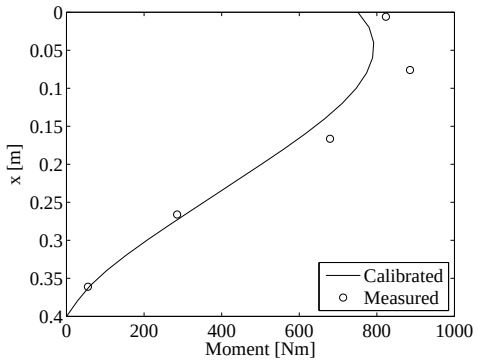

Figure 10: Bending moment distribution determined by means of $FLAC^{3D}$ and the laboratory test result at a horizontal load of 2100 N. $D = 0.08$ m, $L = 0.4$ m, and $P_0 = 100$ kPa.

with $D = 80$ mm, and $P_0 = 100$ kPa have been simulated. The load-displacement relationships are shown in fig. 11.

The load-displacement relationship, cf. fig 11, does not fit the laboratory tests well. In *Plaxis 3D Foundation* a horizontal displacement measured in the level of the hydraulic piston is determined to $y = 13.8$ mm at a horizontal load of $H = 4000$ N. At the same horizontal load a displacement of $y = 8.5$ mm is measured at the laboratory. Hereby, the model in *Plaxis 3D Foundation* overestimates the displacement with approximately 60% compared to the test result.

The potential sources of error causing the

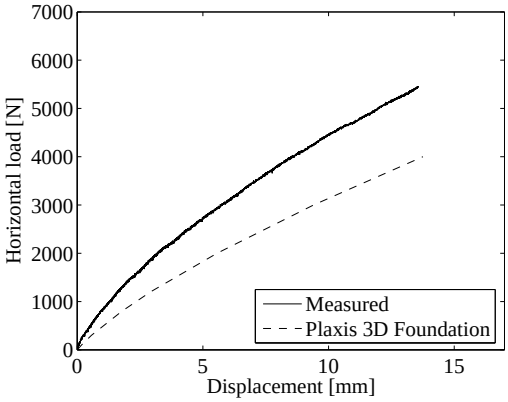

Figure 11: Load-displacement relationship determined by means of *Plaxis 3D Foundation* and laboratory tests, measured at the level of the hydraulic piston. $D = 0.08$ m, $L = 0.4$ m, and $P_0 = 100$ kPa.

large displacements in the *Plaxis 3D Foundation* model are several. The most obvious are the soil parameters including Young's modulus of elasticity of the soil, E_0, and the interface properties. As E_0 governs the initial part of the curve, which is the main focus of this paper, the influence of uncertainties concerning E_0 and the interface properties are evaluated.

The stiffness of the soil is determined from CPT's conducted without overburden pressure and extrapolated under the influence of stress level. If the Young's modulus of elasticity is correct and all other sources of error are negligible, a simulation with an elastic material model should form the tangent stiffness of the laboratory tests. As shown in fig. 12 this is not the case with a Young's modulus of elasticity of $E_0 = 41.0$ MPa as derived from the CPT's. In order to assess the sensitivity of the model with respect to the Young's modulus of elasticity, the impact of doubling the soil stiffness, i.e. $E_0 = 82.0$ MPa, is tested. The load-displacement relationship when doubling E_0 is shown in fig. 12.

Even when doubling the Young's modulus of elasticity the tangent stiffness obtained by means of *Plaxis 3D Foundation*, cf. fig.

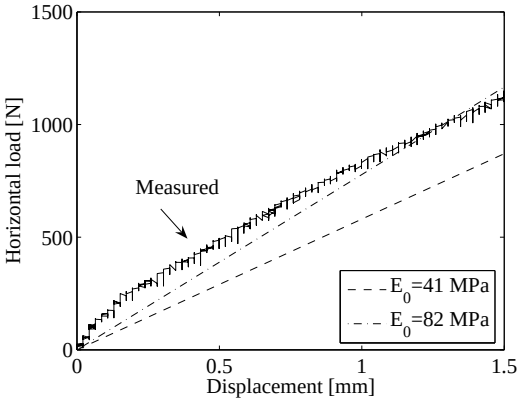

Figure 12: Initial part of load-displacement relationship determined by means of *Plaxis 3D Foundation* when employing an elastic material model. $D = 0.08$ m, $L = 0.4$ m, and $P_0 = 100$ kPa.

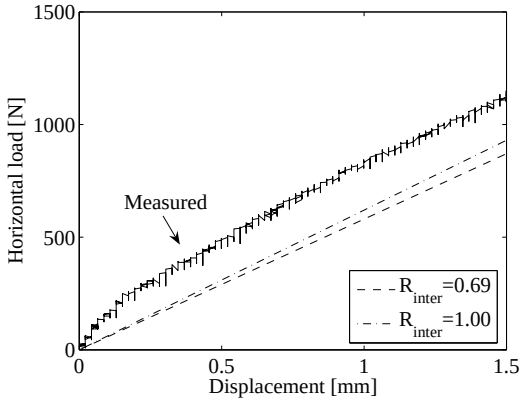

Figure 13: Initial part of load-displacement relationship determined by means of *Plaxis 3D Foundation* when employing R_{inter} of 0.69 and 1.00, respectively. $D = 0.08$ m, $L = 0.4$ m, and $P_0 = 100$ kPa. An elastic material model has been employed.

12, is underestimated compared to the laboratory test. By this it is concluded that the Young's modulus of elasticity is not the main reason for the difference between the results in *Plaxis 3D Foundation* and the laboratory tests.

The interface properties in *Plaxis 3D Foundation* are governed by the parameter R_{inter}. In the simulation shown in fig. 11 a value of $R_{inter} = 0.69$ have been employed after the recommendations in Plaxis 3D Foundation Manual (2007). R_{inter} can maximally take the value $R_{inter} = 1.0$ corresponding to a perfectly rough connection between soil and structure. The effect on the load-displacement relationship of increasing R_{inter} from 0.69 to 1.0 is shown in fig. 13.

A perfectly rough interface between the soil and the pile is highly unlikely. However, the simulation with $E_0 = 41.0$ MPa and $R_{inter} = 1.0$ does not, as shown in fig. 13, result in sufficient stiffness.

The conclusion of the above analysis is that the simulations in *Plaxis 3D Foundation* do not meet an acceptable accuracy for the load-displacement relationship in comparison with the laboratory tests.

4.3 Comparison with a simulation of a Horns Rev monopile

As described, the model in $FLAC^{3D}$ fits the laboratory tests well, which is in contrast to the model in *Plaxis 3D Foundation*. Kellezi and Hansen (2003) have simulated a monopile foundation at Horns Rev subjected to static lateral load. The foundation is subjected to a horizontal load of 2503 kN and a bending moment of 84983 kNm, acting at seabed level. The analysis was performed by means of the three-dimensional numerical program *ABAQUS* assuming drained soil conditions. The soil conditions, cf. tab. 1, are primarily sand with a layer of low-strength organic sand located at a depth of 13.5 m. A Mohr-Coulomb material model incorporating isotropic hardening/softening has been employed by Kellezi and Hansen (2003). The simulation performed by Kellezi and Hansen (2003) is used as benchmark in order to determine whether the numerical model in $FLAC^{3D}$ or the model in *Plaxis 3D Foundation* produce acceptable load-displacement relationships.

Figure 14 presents load-displacement relationships determined by means of

Table 1: Geometric and mechanical data for the soil, after Kellezi and Hansen (2003).

Soil type	Depth [m]	E [kN/m^2]	γ' [kN/m^3]	φ [°]	ψ [°]	ν [-]
Sand	1.0	31800	10	42.0	12.0	0.3
Sand	3.5	57100	10	43.5	13.5	0.3
Sand	5.5	52534	10	42.5	12.5	0.3
Sand	6.5	44100	10	41.7	11.7	0.3
Sand	7.0	58200	10	43.2	13.2	0.3
Sand	8.5	72170	10	44.3	14.3	0.3
Sand	10.0	52950	10	43.1	13.1	0.3
Sand	11.5	35400	10	40.3	10.3	0.3
Sand	12.5	23530	10	37.2	7.2	0.3
Sand	13.5	13600	10	33.8	3.8	0.3
Org. sand	20.0	3135	7	21.6	0.0	0.3
Org. sand	21.04	12950	7	31.2	1.2	0.3
Sand	41.8	36800	10	37.8	7.8	0.3

FLAC^{3D} and *Plaxis 3D Foundation* compared with the results obtained by Kellezi and Hansen (2003). It should be emphasized that similar material parameters and interface properties are employed for the three numerical models. As shown in the figure *Plaxis 3D Foundation* produce a horizontal displacement approximately 99 % larger than *ABAQUS* at a horizontal load of 2503 kN. Hereby, the model in *Plaxis 3D Foundation* overestimates the horizontal displacement compared with both the laboratory tests and the results obtained by *ABAQUS* and *FLAC*^{3D}. The deviation of lateral displacement when comparing the results from *ABAQUS* and *FLAC*^{3D} are small, especially when considering displacements smaller than 0.02 m. The difference between the results obtained by *ABAQUS* and *FLAC*^{3D} at greater displacements might be due to various interface descriptions, and the lack of material hardening incorporated in the *FLAC*^{3D} model.

In order to make a reasonable fit between the load-displacement relationships obtained by means of *ABAQUS* and *Plaxis 3D Foundation* a study on the influence of Young's modulus of elasticity has been performed. When multiplying Young's modulus of elasticity with a factor of 2.5 for all soil layers the difference in pile-head displacement is lower than 2 %, cf. fig. 14, when comparing the results obtained by *ABAQUS* and *Plaxis 3D Foundation*.

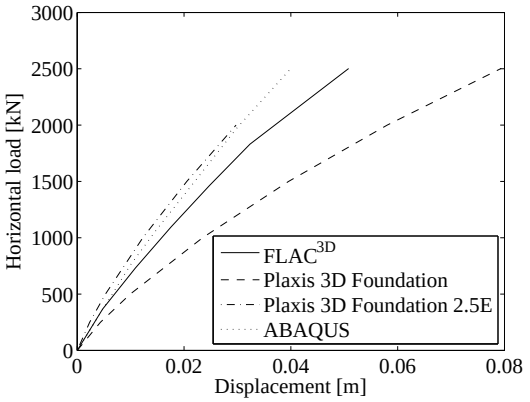

Figure 14: Comparison of load-displacement relationships calculated by means of *FLAC*^{3D} and *Plaxis 3D Foundation* with the results obtained by Kellezi and Hansen (2003) with use of *ABAQUS*.

5 Simulation of large-scale monopiles

In order to evaluate the effects of diameter on the initial stiffness of the p–y curves laterally loaded large-diameter monopiles are simulated by means of the commercial programs *FLAC*^{3D} and *Plaxis 3D Foun-*

dation. In the calibration of the numerical models *Plaxis 3D Foundation* were found to overestimate the pile deflection in comparison with the laboratory tests. Furthermore, *Plaxis 3D Foundation* also produced a larger displacement when simulating the load-displacement relationship for a monopile at Horns Rev compared to numerical models in *ABAQUS* and $FLAC^{3D}$. Therefore, *Plaxis 3D Foundation* is not expected to produce realistic values of soil resistance and pile deflection. However, a realistic variation of soil resistance with pile diameter and depth have been observed in the calibrations. The model is therefore employed in the simulation of large-scale monopiles in order to validate the tendencies observed in $FLAC^{3D}$. *Plaxis 3D Foundation* is much less time consuming than $FLAC^{3D}$ implying the possibility of more simulations at a given time period.

In the evaluation of the effects of diameter on the initial stiffness of the p–y curves, four circular, closed-ended, pipe piles with diameters of 2 m, 3 m, 5 m, and 7 m are simulated in both $FLAC^{3D}$ and *Plaxis 3D Foundation*. Furthermore, a slender monopile with a diameter of 1 m are simulated in *Plaxis 3D Foundation*. The pile with this diameter has not produced a realistic load-displacement relationship by means of $FLAC^{3D}$ due to a high load eccentricity compared to the pile diameter. All piles have a wall thickness of 0.05 m and the horizontal load is applied with a vertical eccentricity of 15 m. The embedded length of the piles is 20 m, except for the analyses conducted in section 5.6. For all analyses drained soil conditions are employed.

5.1 Soil and pile properties at large-scale analyses

The material parameters for the soil and the piles employed in the simulations are given in tab. 2. The material properties of the large-scale piles corresponds to the properties of steel and are scaled in accordance to (1). The tangential Young's modulus of elasticity, E_0, is varied with depth, cf. (2)-(3).

5.2 Effects of diameter on pile behaviour

Figure 15 presents the lateral pile deflection behaviour with respect to depth for the model incorporated in $FLAC^{3D}$. The applied displacements at the pile-head, corresponding lateral loads, and depth of maximum moments are outlined in tab. 3. As shown the lateral displacements at the pile-head and the horizontal loads are different in the four cases. The more rigid pile behaviour for increasing diameters, cf. fig. 15, is in good accordance with Poulus and Hull (1989) as the employed pile bending stiffness increases for increasing pile diameter. Due to the rigid pile behaviour, a significant negative deflection is observed at the pile-toe. The magnitude of negative deflection increases with increasing pile bending stiffness. The point of zero deflection, cf. fig. 15, are for $D = 3-7$ m located at a depth of approximately $x = 15$ m at the applied displacements, cf. tab. 3. As the pile deflection for $D = 2$ m consists of a high amount of deformation due to bending the point of zero deflection is located nearer the soil surface at a depth of approximately $x = 13$ m. For all piles it has been observed that the location of the point of zero deflection depends on the applied displacement; the distance measured from soil surface to the depth of zero deflection increases with increasing displacement. This is caused by the fact that the zone of failure propagates downwards with increasing pile displacement.

The distribution of bending moments with depth simulated in $FLAC^{3D}$ are presented in fig. 16. It is observed that the maximum bending moment is located at depths of approximately 5 m for $D = 3-7$ m. For $D = 2$ m the maximum bending moment

Table 2: Material properties employed for the large-scale analyses.

Unit weight of the soil γ'	10 kN/m^3
Angle of internal friction φ_{tr}	40°
Dilatancy angle ψ_{tr}	10°
Cohesion c	0.1 kN/m^2
Relative density I_D	80%
Poisson's ratio for the soil ν_s	0.23
Coefficient of horizontal earth pressure at rest K_0	1-sin(φ_{tr})
Young's modulus of elasticity for the hollow pile E_p	210 GPa
Poisson's ratio for the pile ν_p	0.3
Unit weight of the pile γ_p	78.5 kN/m^3

Table 3: Applied displacements at the pile-head, equivalent loads, and depth of maximum moments for the analyses in $FLAC^{3D}$.

Outer pile diameter [m]	Displacement [m]	Load [MN]	Depth of max. moment [m]
2	0.49	2.5	4.5
3	0.58	6.4	4.8
5	0.24	8.8	5.0
7	0.84	21.4	4.9

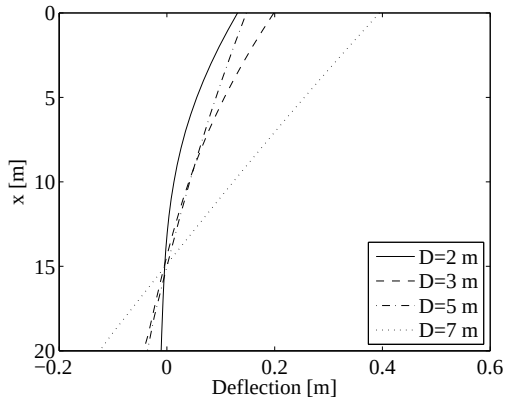

Figure 15: Lateral pile deflection calculated by means of $FLAC^{3D}$.

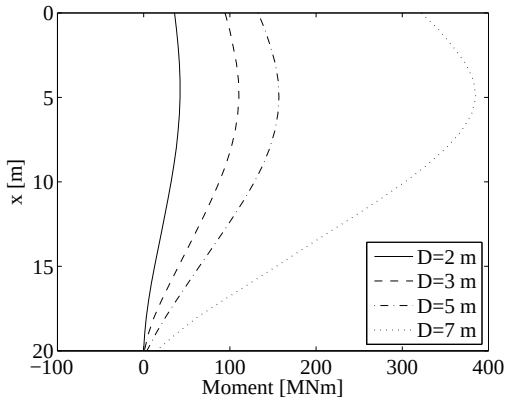

Figure 16: Bending moment distribution calculated by means of $FLAC^{3D}$.

is located at a depth of approximately 4.5 m. As the point of zero deflection for the pile with $D = 2$ m is located nearer the soil surface than for the other three piles, the maximum moment is also expected to be located nearest to the soil surface.

A similar pile behaviour has been observed for the model constructed in *Plaxis 3D Foundation*. The pile with $D = 1$ m deflects primarily by bending resulting in almost zero horizontal displacement at the pile-toe.

5.3 Comparison of computed p–y curves with the design regulations

The distribution of soil resistance with depth for the model in $FLAC^{3D}$ is shown in fig. 17. It is observed that the soil resistance do not approach zero at the soil surface for all piles. However, it should be emphasized that the soil resistance at the soil surface is approximated from the bending moment at the soil surface and at

four points below the soil surface. Hereby, uncertainties are attached to the determination of the soil resistance at the soil surface. These uncertainties also account for the calculated soil resistance at the pile-toe. Alternatively the soil resistance could have been computed by integrating the stresses in the interface elements along the circumference of the pile. Deviations in the soil resistance can be observed near the point of zero deflection, most significantly for $D = 7$ m. Small uncertainties in the bending moment distribution implies uncertainties when determining the soil resistance. Near the point of zero deflection the soil resistance is approximately zero and the effect of uncertainties on the distribution of soil resistance is therefore most significant at this depth.

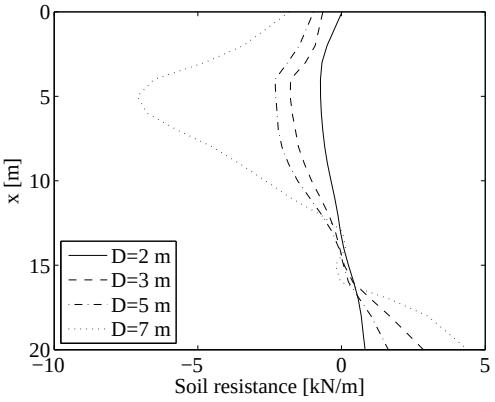

Figure 17: Soil resistance versus depth determined by means of $FLAC^{3D}$.

Figure 18 presents the p–y curves obtained by means of $FLAC^{3D}$ at a depth of $x = 2$ m. Further, the p–y curves according to the design regulations, e.g. API (1993) and DNV (1992), are outlined in the figure. As expected the ultimate soil resistance increases with increasing pile diameter. Further, the initial part of the curves, is stiffer for the API p–y curves compared to the p–y curves obtained by means of $FLAC^{3D}$. The ultimate soil resistance of the API p–y curves has some degree of conservatism in the case of very large diameters. This is however, not observed for the piles with $D = 2 - 3$ m. Furthermore, the p–y curves obtained from the three-dimensional numerical model do not reach a steady state at the applied displacements. Although the load-displacement relationship obtained by a force and a displacement controlled approach are in agreement, cf. fig. 4, the p–y curve for $D = 2$ m has some degree of fluctuation.

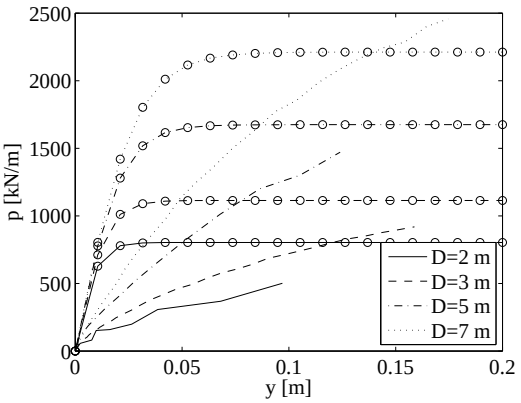

Figure 18: Comparison of API p–y curves marked with (o) and the p–y curves obtained by means of $FLAC^{3D}$ for the four piles, respectively.

5.4 Variation of initial stiffness with depth

The variation of initial stiffness with depth, $E^*_{py} = \frac{dp}{dy}$, $y = 0$, is presented in fig. 19a for the four pile diameters modelled in $FLAC^{3D}$. Figure 19b presents the variation of E^*_{py} with depth for the analyses computed by means of *Plaxis 3D Foundation*. From the figures it is observed that the initial stiffness increases with increasing pile diameter. The offshore design regulations, e.g. DNV (1992) and API (1993), suggest that the initial modulus of subgrade reaction, k, and hereby also the initial stiffness $E^*_{py} = kx$:

$$\frac{dp}{dy} \mid_{y=0} = Ap_u \frac{\frac{kx}{Ap_u}}{\cosh^2(\frac{kxy}{Ap_u})} \mid_{y=0} = kx \quad (6)$$

is independent of the pile diameter. This is in contrast to the variation of initial stiffness with depth shown in fig. 19a and fig.

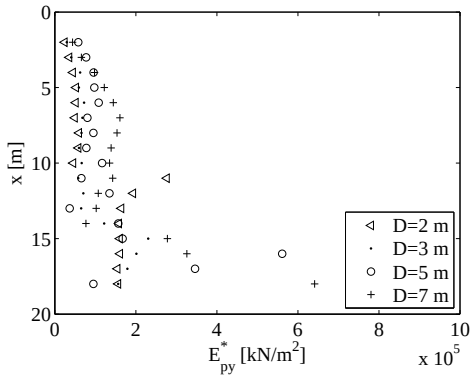

(a) *FLAC*^{3D}.

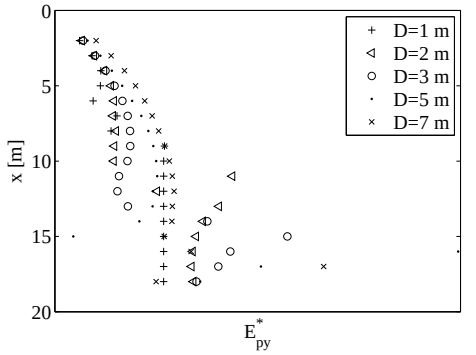

(b) *Plaxis 3D Foundation.*

Figure 19: Initial stiffness, E^*_{py}, versus depth.

19b. The p–y curves obtained near the point of zero deflection as well as at the pile-toe is characterised by a lot of scatter due to small deflections causing large uncertainties for the initial stiffness at large depths.

According to fig. 19a and fig. 19b E^*_{py} does not vary linearly with depth. Lesny and Wiemann (2006) propose a power function for the variation of E^*_{py} with depth:

$$E^*_{py} = E^*_{py,ref} \left(\frac{x}{x_{ref}} \right)^a \qquad (7)$$

where $E^*_{py,ref}$ denotes the initial stiffness at a reference depth, x_{ref}, and a is a factor depending on the relative density of the sand. According to Lesny and Wiemann (2006) the factor a is to be set to 0.6 for medium dense sands.

Figure 20 presents the initial stiffness' obtained by means of *Plaxis 3D Foundation* and the variations based on (6) and (7) for $D = 7$ m. The two expressions, cf. (6) and (7), are identical when $a = 1$. As a reference initial stiffness, $E^*_{py,ref}$, the initial stiffness at $x_{ref} = 2$ m is employed. Figure 20 indicate that the linear expression employed in the design regulations fits the obtained E^*_{py} well until a depth of approximately 5 m. Beneath this depth the linear expression highly overestimates E^*_{py}, given that the soil response is non-conservative at large depths. Equation (7) fits the obtained E^*_{py} very well until a depth of 14 m. Equation (6) is highly affected by the value of k while (7) produces a reasonable fit independent of the reference value due to the non-linear behaviour. E^*_{py} is not clearly defined beneath $x = 14$ m due to the influence of the point of zero deflection. For the remaining pile diameters a similar non-linear variation of E^*_{py} with depth is found, most significantly for $D = 3 - 7$ m. Hereby, the expression in the offshore design regulations overestimates the soil-pile interaction for large-diameter monopiles at large depth. The non-linear variation of initial stiffness is observed in connection with both the analyses in *FLAC*^{3D} and *Plaxis 3D Foundation*.

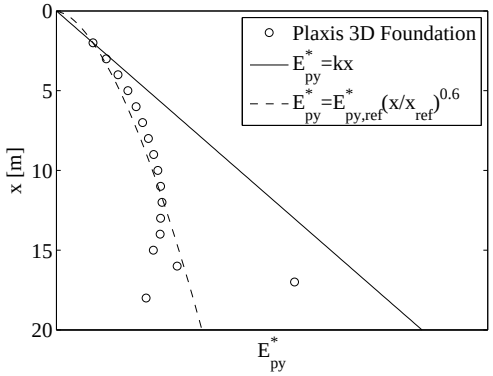

Figure 20: Variation of E^*_{py} as function of depth determined by means of *Plaxis 3D Foundation* for $D = 7$ m, and $x_{ref} = 2$ m.

5.5 Effect of diameter on initial modulus of subgrade reaction

The magnitudes of k in (6) obtained by means of *FLAC*^{3D} are outlined in tab. 4 at $x = 2 - 7$ m where the assumption of a linear variation of initial stiffness with depth is reasonable. As indicated in tab. 4, k is highly dependent on the pile diameter; increasing diameter results in an increase in k. This observation is most significant when comparing the results for the piles with $D = 2 - 5$ m. For dense sand ($\varphi_{tr} = 40°$) the offshore design regulations recommend $k = 40000$ kN/m^3. This does not agree with the analyses since k ranges between 7000–29000 kN/m^3.

A power function of the form:

$$k = k_{ref} \left(\frac{D}{D_{ref}} \right)^b \tag{8}$$

is employed in order to describe the relation between k and D.

Figure 21 and 22 presents the normalised relationship based on (8) by means of the two numerical models, respectively. The exponent b is determined to 0.645 and 0.226 by means of *FLAC*^{3D} and *Plaxis 3D Foundation*, respectively. Hereby, there is a considerable difference between k/k_{ref}, cf. fig. 21 and 22, obtained by the two numerical models. This difference is most significant at diameters of $D = 5-7$ m implying a higher exponent b determined by means of *FLAC*^{3D}. However, both models highly indicates that there is a correlation between k and D. More research is needed in order to make a clear correlation between pile diameter and initial modulus of subgrade reaction.

5.6 Effect of extra embedded length

The previous analyses have been based on varying diameters and a constant embedded pile length of 20 m. In order to eliminate the effect of embedded length on the initial stiffness of the p–y curves the embedded length has been extended to 30 m. The analyses have been made by means of *Plaxis 3D Foundation*. Figure 23 presents the variation of E^*_{py} with depth when varying the embedded length for $D = 3$ m and $D = 5$ m, respectively. From fig. 23 it is observed that E^*_{py} is not significantly influenced by the embedded length. The point of zero deflection changes slightly with length. Due to an extra embedded length reasonable p–y curves beneath the point of zero deflection is obtained. Similar results have been obtained for the remaining pile diameters.

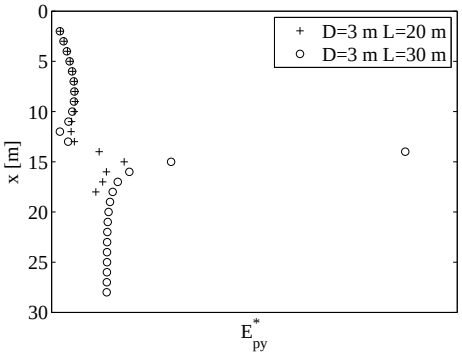

(a) $D = 3$ m.

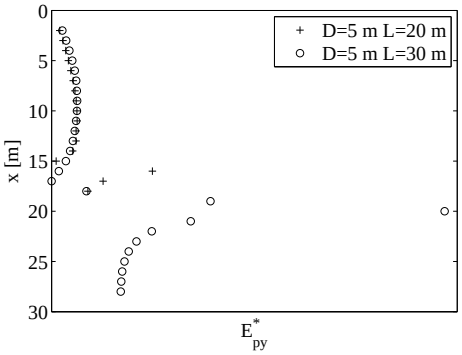

(b) $D = 5$ m.

Figure 23: Effect of embedded length on E^*_{py} determined by means of *Plaxis 3D Foundation*.

Table 4: Initial modulus of subgrade reaction, k, obtained by means of $FLAC^{3D}$. k is specified in [kN/m^3].

	$D = 2$ m	$D = 3$ m	$D = 5$ m	$D = 7$ m
$x = 2$ m	12116	14799	28964	21891
$x = 3$ m	11899	13550	25798	21846
$x = 4$ m	11166	15663	23921	24547
$x = 5$ m	10482	11881	19532	24440
$x = 6$ m	8602	12045	18065	24077
$x = 7$ m	7051	9747	11475	22963

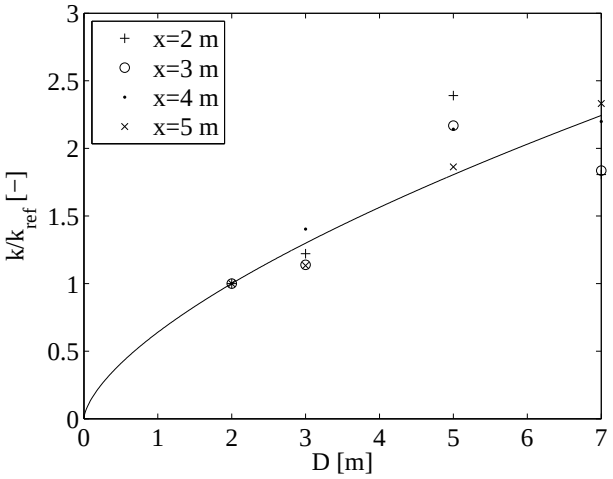

Figure 21: Normalised initial modulus of subgrade reaction versus pile diameter determined by means of $FLAC^{3D}$. As k_{ref} the value at $D = 2$ m have been employed. $b = 0.645$.

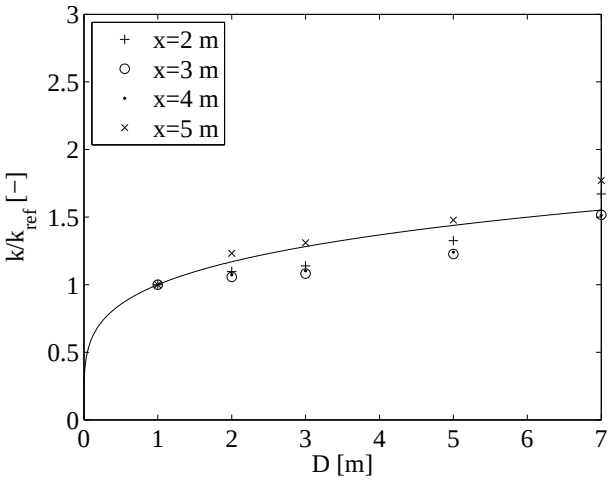

Figure 22: Normalised initial modulus of subgrade reaction versus pile diameter determined by means of *Plaxis 3D Foundation*. As k_{ref} the value at $D = 1$ m have been employed. $b = 0.226$.

5.7 Variation of pile bending stiffness

According to Ashour and Norris (2000) the bending stiffness of the pile, E_pI_p, has significant influence on the p–y curves. In order to investigate whether the changes in E^*_{py} registered for different pile diameters are related to the bending stiffness of the pile, simulations have been performed in *Plaxis 3D Foundation* with varying values of E_pI_p. The evaluation has been carried out for $D = 3$ m. The second moment of inertia, I_p, has, due to a constant geometry, been kept constant. Young's modulus of elasticity for the hollow pile has been varied between the values $E_p = 2.1 \cdot 10^7$ kPa, $E_p = 2.1 \cdot 10^8$ kPa, and $E_p = 2.1 \cdot 10^9$ kPa. Figure 24 presents derived p–y curves when varying the pile bending stiffness determined by means of *Plaxis 3D Foundation*. The figures outline the derived p–y curves at a depth of $x = 2$ m and $x = 10$ m, respectively.

As shown in fig. 24 the pile bending stiffness does not have significant influence on the p–y curves, neither on the initial stiffness nor on the ultimate soil resistance. This investigation is substantiated by the work performed by Fan and Long (2005). The point of zero deflection is situated nearer the soil surface when decreasing the pile bending stiffness. Due to this, the most slender pile is characterised by a lot of scatter at $x = 10$ m, cf. fig. 24b.

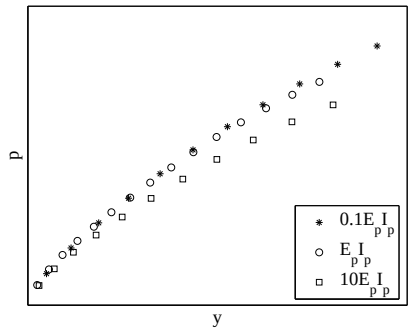

(a) $x = 2$ m

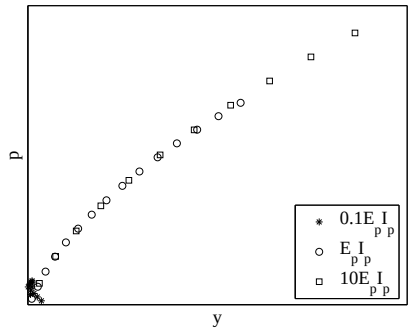

(b) $x = 10$ m

Figure 24: p–y curves determined for different pile bending stiffness' by means of *Plaxis 3D Foundation*. $D = 3$ m.

5.8 Load-displacement relationships

Based on small-scale tests Sørensen et. al indicate that the horizontal load is proportional to the embedded length squared and the pile diameter. However, it should be emphasised that the slenderness ratio, L/D, were kept constant for all tests.

Figure 25 presents normalised load-displacement relationships for various pile diameters and embedded lengths calculated by means of *Plaxis 3D Foundation*. The horizontal load is normalised as $H/L^2D\gamma$ and the pile displacement as y/D. A disagreement between the normalised load-displacement relationships for the various simulated piles can be observed.

As a constant slenderness ratio were employed for the small-scale tests, the lateral load might as well be proportional to the embedded length and the pile diameter squared. Figure 26 show the normalised relationships between load, $H/LD^2\gamma$, and displacement, y/D, at the pile-head for various pile diameters and embedded lengths. A good agreement can be observed for the normalised load-displacement relationships of the various piles. Hereby, the simulations in *Plaxis 3D Foundation* indicate a proportionality be-

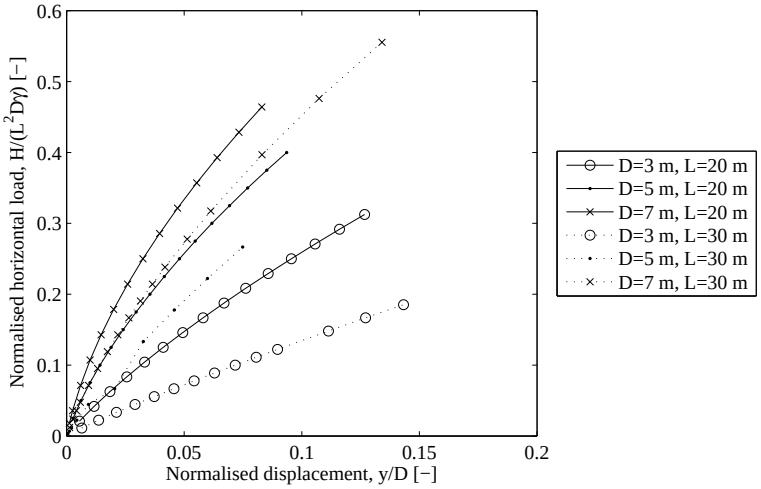

Figure 25: Normalised relationships between load ($H/L^2D\gamma$) and displacement (y/D) determined at the pile-head at various pile diameters and embedded lengths by means of *Plaxis 3D Foundation*.

tween the lateral load and the embedded length and the pile diameter squared.

6 Comparison of *FLAC*^{3D} with a Winkler model approach

A traditional Winkler model has been constructed in order to compare the results obtained from the three-dimensional numerical model in *FLAC*^{3D} with the recommendations in the design regulations, e.g. API (1993) and DNV (1992). The non-linear soil-pile interaction is modelled using the API (1993) p–y curves. Bernoulli-Euler beam theory is employed for the pile. The comparison between the results obtained by means of *FLAC*^{3D} and the Winkler model approach is performed, with the same pile geometry, and soil conditions as listed in tab. 2. In fig. 27 the pile deflection with depth obtained by means of *FLAC*^{3D} and the Winkler model, respectively, is compared for an applied horizontal load at the pile-head of 6.4 MN for $D = 3$ m. The lateral pile deflection determined by means of *FLAC*^{3D} indicate a very stiff pile behaviour compared to the pile behaviour obtained by the Winkler model approach incorporating API p–y curves, cf. fig. 27. Further, some conclusions can be drawn:

- The deflection at the soil surface determined by means of the Winkler model approach is 37 % of the deflection computed by means of *FLAC*^{3D}.
- The deflection at the pile-toe determined by means of the Winkler model approach is 4 % of the deflections computed by means of *FLAC*^{3D}.
- The point of zero deflection is situated at a depth of approximately 11.0 m for the Winkler model approach. By means of *FLAC*^{3D} the point of zero deflection is situated in a depth of approximately 14.4 m.

The large disagreement for the pile deflection at the pile-toe indicates that the soil resistance is highly overestimated in the design regulations at large depths. The overestimation of soil resistance at large depths also causes the disagreement in the location of the point of zero deflection.

In fig. 28 the bending moment distribution along the pile obtained by means of

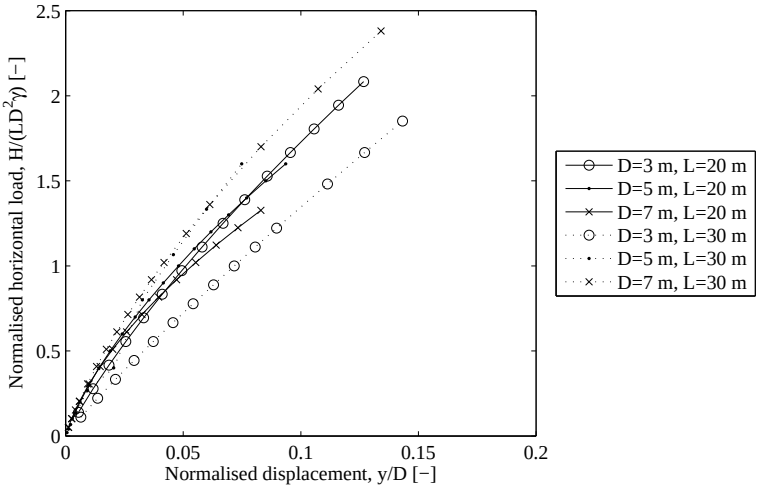

Figure 26: Normalised relationships between load ($H/LD^2\gamma$) and displacement (y/D) determined at the pile-head at various pile diameters and embedded lengths by means of *Plaxis 3D Foundation*.

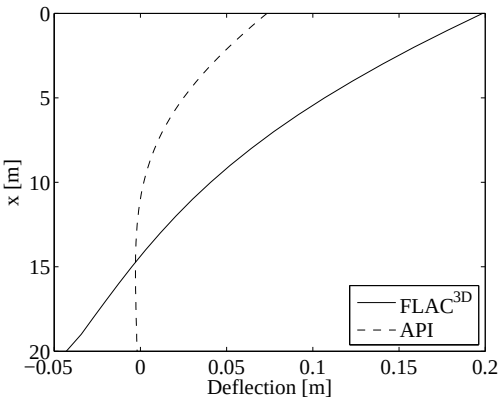

Figure 27: Comparison of lateral pile deflection calculated by means of $FLAC^{3D}$ with the Winkler model approach employing API p–y curves for $D = 3$ m.

$FLAC^{3D}$ and the Winkler model, respectively, is compared for an applied horizontal load of 6.4 MN for $D = 3$ m. A reasonable agreement between the distribution of bending moment for the model in $FLAC^{3D}$ and the Winkler model can be observed. The depth of maximum bending moment is for both models located at a depth of approximately 5 m. The Winkler model approach overestimates the size of the maximum bending moment with 5 % compared to $FLAC^{3D}$. Near the pile-toe the bending moment computed by means of $FLAC^{3D}$ varies almost linearly with depth. This is in contrast to the bending moment calculated by means of the Winkler model approach, where a significantly non-linear variation of bending moment with depth is observed. As the soil resistance is determined as the 2. order derivative of the bending moment the significant non-linear variation of bending moment at large depths indicate a large soil resistance. Hereby, the distribution of bending moment substantiate the observations in fig. 27.

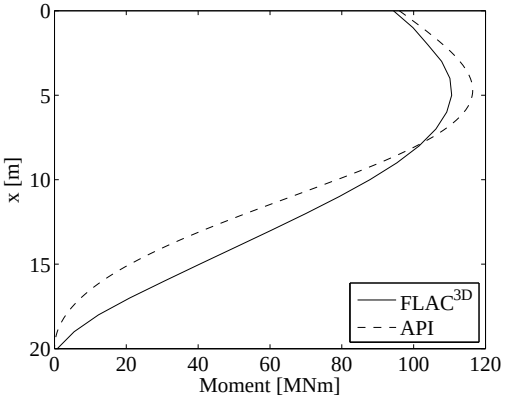

Figure 28: Comparison of bending moment distribution calculated by means of $FLAC^{3D}$ with the Winkler model approach employing API p–y curves for $D = 3$ m.

Figure 29 presents the load-displacement relationships at the pile-head located 15 m

above seabed ($D = 3$ m) obtained by means of $FLAC^{3D}$ and the Winkler model approach. The power function, cf. (7), and the recommendations in API (1993), with $k = 40000$ kN/m^3 and $k = k_{ref}$ at $x = 2$ m, respectively have in turn been implemented in the Winkler model approach. Figure 29 indicate that the expression employed in API (1993) highly overestimates the strength of the soil at all deflections compared to $FLAC^{3D}$. This is expected in accordance with tab. 4 since the initial modulus of subgrade reaction, k, recommended by API (1993) is overestimated compared to the values calculated by means of FLAC^{3D}. The linear expression, cf. (6), with k_{ref} as the value obtained at $x_{ref} = 2$ m produces reasonable results until a deflection of approximately 0.1 m. At greater deflections there is a considerable difference between the deflections determined by $FLAC^{3D}$ and the linear expression. When employing the power function, cf. (7), in the Winkler model approach the initial part of the load-displacement relationship fits very well until a deflection of 0.2 m. At greater deflections an overestimation of the horizontal load is observed compared to $FLAC^{3D}$. However, the difference is much smaller than obtained by employing the linear expression in the Winkler model. Similar load-displacement behaviour has been observed for the remaining pile diameters.

For modern wind turbine foundations only small deformations/rotations are allowed. Therefore, it is desirable that the initial part of the curves fits the pile behaviour well, which is the case for the power function employed in the Winkler model approach. Hence, it can be concluded that the Winkler model approach is useful when a proper variation of the initial stiffness associated with the p–y curves is employed.

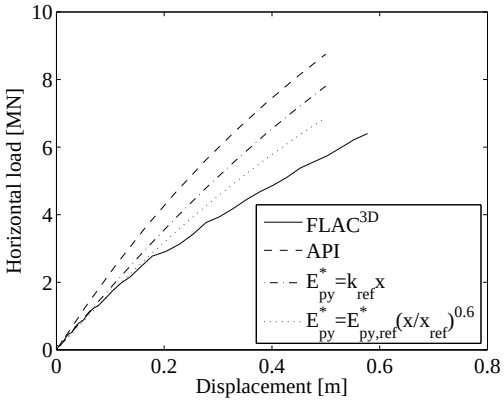

Figure 29: Load-displacement relationships at the pile-head calculated by means of $FLAC^{3D}$ compared with the Winkler model approach incorporating API ($k = 40000$ kN/m^3), API (k_{ref}), and the power function, cf. Lesny and Wiemann (2006), respectively.

7 Conclusion

A numerical study of the behaviour of laterally loaded large-diameter monopiles in sand is presented in this paper. The evaluation is made by means of the three-dimensional numerical programs $FLAC^{3D}$ and *Plaxis 3D Foundation*. The numerical models are calibrated against well-defined small-scale tests and hereafter extended to large-scale monopiles with pile diameters varying between $D = 2 - 7$ m. During the calibration process, *Plaxis 3D Foundation* were found to overestimate the pile deflection in comparison with the laboratory tests. Therefore, *Plaxis 3D Foundation* does not produce realistic values of soil resistance and pile deflection. However, a realistic variation of soil resistance with pile diameter and depth were observed. The model were therefore employed in the simulation of large-scale monopiles in order to validate the tendencies observed in $FLAC^{3D}$. The conclusions that can be drawn are:

- Non-slender piles deflect as almost rigid objects resulting in only one point of zero deflection. Hence, significant negative deflections at the pile-

toe are observed.

- The initial modulus of subgrade reaction, k, is highly affected by the pile diameter; increasing diameter results in an increase in k. This is observed in both *FLAC*^{3D} and *Plaxis 3D Foundation* simulations. This contradicts the recommendations in the offshore design regulations. k is varying between 7000–29000 kN/m^3 at small depths when increasing the diameter from 2–7 m.
- The initial stiffness of the p–y curves, E^*_{py}, is independent of both the embedded length of the pile and the pile bending stiffness, E_pI_p. According to this, the main parameter affecting E^*_{py} is the pile diameter.
- The design regulations recommends a linear variation of initial stiffness with depth. This recommendation is non-conservative at large depths. Here, the soil response is overestimated. A non-linear variation of initial stiffness with depth proposed by Lesny and Wiemann (2006) provides a good agreement when compared to the results from the three-dimensional numerical analyses.
- The numerical analyses indicate that the horizontal load acting at the pile-head is proportional to the pile diameter squared and the embedded pile length.

Acknowledgements

The project has only been possible with the financial support from the Energy Research Programme administered by the Danish Energy Authority. The project is associated with the EFP programme "Physical and numerical modelling of monopile for offshore wind turbines", journal no. 033001/33033-0039. The funding is sincerely acknowledged.

References

Abbas J. M., Chik Z. H., and Taha M. R., 2008. Single Pile Simulation and Analysis Subjected to Lateral Load. *Electronic Journal of Geotechnical Engineering*, **13E**, pp. 1-15.

API, 1993. Recommended practice for planning, designing, and constructing fixed offshore platforms - Working stress design, *API RP2A-WSD*, American Petrolium Institute, Washington, D.C., 21. edition.

Ashour M., and Norris G., May 2000. Modeling lateral soil-pile response based on soil-pile interaction. *Journal of Geotechnical and Geoenvironmental Engineering*, **126**(5), paper no. 19113, pp. 420-428.

Brødbæk K. T., Møller M., and Sørensen S. P. H., 2009. Review of p–y Relationships in Cohesionless Soil. *DCE Technical Report no. 57*, Department of Civil Engineering, Aalborg University, Denmark.

Cox W. R., Reese L. C., and Grubbs B. R., 1974. Field Testing of Laterally Loaded Piles in Sand. *Proceedings of the Sixth Annual Offshore Technology Conference*, Houston, Texas, paper no. OTC 2079.

DNV, 1992. Foundations - Classification Notes No 30.4, Det Norske Veritas, Det Norske Veritas Classification A/S.

Fan C. C., and Long J. H., 2005. Assessment of existing methods for predicting soil response of laterally loaded piles in sand. *Computers and Geotechnics* **32**, pp. 274-289.

FLAC^{3D} 3.1 manual, 2006. Fast Lagrangian Analyis of Continua in 3 Dimensions, Itasca Consulting Group Inc., Minneapolis, Minnesota, USA.

Ibsen L. B., Hanson M., Hjort T. H., and Thaarup M., 2009. MC–Parameter Calibration for Baskarp Sand No. 15. *DCE*

Technical Report No. 62, Department of Civil Engineering, Aalborg University, Denmark.

Kellezi L., and Hansen P. B., 2003. Static and dynamic analysis of an offshore mono-pile windmill foundation. *Proceedings of the BGA International Conference on Foundations: Innovations, observations, design and practice*, Dundee, UK, pp. 401-410.

Lesny K., and Wiemann J., 2006. Finite-Element-Modelling of Large Diameter Monopiles for Offshore Wind Energy Converters. *Geo Congress 2006, February 26 to March 1*, Atlanta, GA, USA.

Plaxis 3D Foundation Manual Version 2, Brinkgreve R. B. J., and Swolfs W. M. (edt.), 2007.

Poulus H., and Hull T., 1989. The Role of Analytical Geomechanics in Foundation Engineering. *in Foundation Eng.: Current principles and Practices*, **2**, pp. 1578-1606.

Sørensen S. P. H., Møller M., Brødbæk K. T., Augustesen A. H., and Ibsen L. B., 2009. Evaluation of Load-Displacement Relationships for Non-Slender Monopiles in Sand. *DCE Technical Report no. 79*, Department of Civil Engineering, Aalborg University, Denmark.

Yang K., Liang R., 2006. Methods for Deriving *p–y* Curves from Instrumented Lateral Load Tests. *Geotechnical Testing Journal*, **30**(1), paper ID GTJ100317, pp. 31-38.

Appendix

The test programme and material properties for the soil and piles are given in tab. 5. For the tests without overburden pressures Young's modulus of elasticity of the soil is calibrated as the low horizontal stresses leads to large uncertainties. For all analyses the Poisson's ratio is $\nu_p = 0.33$ and $\nu_s = 0.23$, for the piles and soil, respectively. In $FLAC^{3D}$ the interface shear stiffness and interface normal stiffness is set to $k_s = k_n = 100E_0$.

Table 5: Test programme and material properties for the six tests.

	Diameter	Overburden pressure	Angle of internal friction	Dilatancy angle	Cohesion	Relative density	Unit weight	Young's modulus of elasticity	Pile bending stiffness
	D [m]	P_0 [kPa]	φ_{tr} [°]	ψ [°]	c [kPa]	I_D [–]	γ' [kN/m^3]	E_0 [MPa]	E_pI_p [kNm^2]
Test 1	0.8	0	52.6	10	0.1	0.79	10.2	-	52.4
Test 2	0.8	100	45.9	10	0.1	0.79	10.2	41.1	52.4
Test 3	0.8	50	48.5	10	0.1	0.79	10.2	25.4	52.4
Test 4	0.6	0	52.2	10	0.1	0.76	10.1	-	24.9
Test 5	0.6	50	48.3	10	0.1	0.78	10.1	24.9	24.9
Test 6	0.6	100	45.1	10	0.1	0.75	10.1	37.4	24.9

ISSN 1901-726X
DCE Technical Report No. 80